NASA TECHNICAL NOTE

NASA TN D-5288

c. 1

NASA TN D-5288

ANALYSIS OF TWO DIMENSIONAL INVISCID MODEL OF JET IMPINGEMENT UNDER VERTICAL-TAKEOFF AIRPLANE

by Robert Siegel and Marvin E. Goldstein

Lewis Research Center
Cleveland, Ohio

NATIONAL AERONAUTICS AND SPACE ADMINISTRATION • WASHINGTON, D. C. • JUNE 1969

ANALYSIS OF TWO DIMENSIONAL INVISCID MODEL OF JET IMPINGEMENT UNDER VERTICAL-TAKEOFF AIRPLANE

By Robert Siegel and Marvin E. Goldstein

Lewis Research Center
Cleveland, Ohio

NATIONAL AERONAUTICS AND SPACE ADMINISTRATION

For sale by the Clearinghouse for Federal Scientific and Technical Information
Springfield, Virginia 22151 – CFSTI price $3.00

ABSTRACT

Conformal mapping was used to obtain the free streamline pattern and surface pressure distribution for downward jet flow issuing from two parallel slot nozzles. After striking the ground, a portion of the flow from each jet moves along the ground toward the centerline between the jets. When these two portions collide, an upflow results which strikes a plate above the ground simulating the undersurface of an airplane fuselage. Typical flow patterns are shown to illustrate the effect on the free streamlines of nozzle height, nozzle spacing, plate height, plate width, and plate angle.

ANALYSIS OF TWO DIMENSIONAL INVISCID MODEL OF JET IMPINGEMENT UNDER VERTICAL-TAKEOFF AIRPLANE

by Robert Siegel and Marvin E. Goldstein

Lewis Research Center

SUMMARY

Conformal mapping was used to obtain the free streamline pattern and surface pressure distribution for downward jet flow issuing from two parallel slot nozzles. After striking the ground, a portion of the flow from each jet moves along the ground toward the centerline between the jets. When these two portions collide, an upflow results which strikes a plate above the ground simulating the undersurface of an airplane fuselage. Typical flow patterns are shown to illustrate the effect on the free streamlines of nozzle height, nozzle spacing, plate height, plate width, and plate angle.

INTRODUCTION

Under a vertical-takeoff (VTOL) airplane, as illustrated by figure 1, there is a complicated flow pattern. The downward directed jets in figure 1(b), react against the ground, and a portion of the flow is turned outward and flows along the ground. The remaining flow moves inward, and under the fuselage the opposing streams collide and move upward. Portions of this upward flow will move around the fuselage or will recirculate under the wings. The upward flow in some instances provides a useful lifting force. However, it is generally undesirable because of recirculation of hot exhaust gases around portions of the airplane. This recirculating flow may be partially ingested into the engines, along with dust and debris from the ground that has been entrained (refs. 1 and 2).

The complicated interaction with the ground and the airplane, and the presence in many instances of turbulent mixing, makes the analytical prediction of the three-dimensional flow flow field under a vertical-takeoff airplane extremely difficult. To obtain analytical solutions a simplified incompressible, isothermal flow model is employed herein that retains some of the major features of the actual flow field. The analysis is

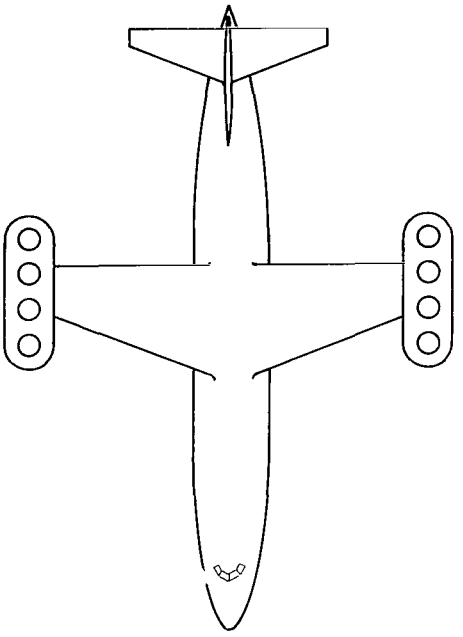

(a) Plan view of airplane.

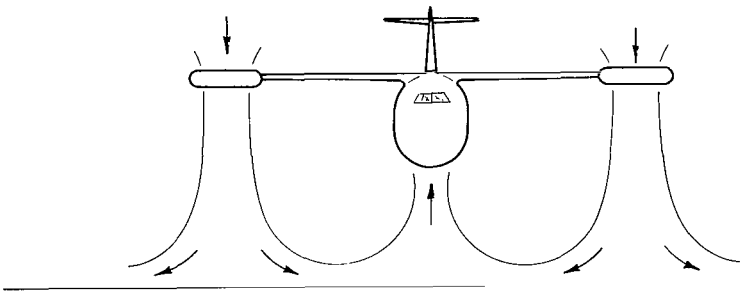

(b) Flow pattern under airplane.

CD-10386-02

Figure 1. - Flow configuration for fan-pod VTOL aircraft.

an extension of that in reference 3. As shown in figure 1, a fan-pod type of configuration is being considered. A two-dimensional approximation will be made to study the flow in the region between the engines. The flow is assumed to be inviscid; this could be approximately true when the nozzle exit planes are within a few nozzle widths of the ground and within a few widths apart. For these conditions there will be only a small entrainment of surrounding fluid into the jet region prior to the flow being turned by the ground and turned under the fuselage. The two-dimensional model is shown in figure 2. A plate, which can be at an angle to the ground, has been used to simulate each half of the undersurface of the fuselage.

By using a two-dimensional inviscid model, the determination of the flow field

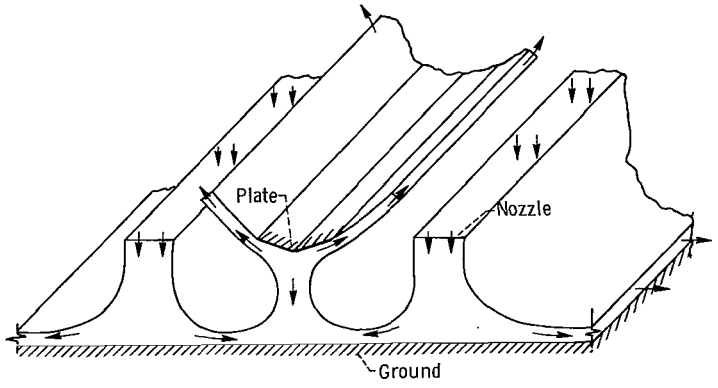

Figure 2. - Two-dimensional model of jet deflection by ground and fuselage.

becomes a free streamline problem in constant pressure surroundings. A solution can be obtained by using the Helmholtz-Kirchhoff method (ref. 4). This conformal mapping procedure is used to find a functional relation between the complex conjugate velocity and the complex potential of the flow. Then the flow configuration is obtained by integrating the complex potential multiplied by the reciprocal of the complex conjugate velocity.

The flow pattern depends on the flow condition leaving the nozzle. The condition assumed herein is that the flow leaves perpendicular to the nozzle exit plane. This is a reasonable condition for nozzles of small width or when turning vanes are used to guide the flow. The interaction of the flow with the ground produces a nonuniform downward velocity leaving the nozzle; the velocity in the central region of the nozzle exit plane is less than that along the nozzle sides.

The final analytical results were evaluated for several combinations of the parameters, such as plate height, plate width, and spacing between nozzles. Typical free streamline flow patterns are given along with the pressure coefficient along the plate, and the velocity distribution across the nozzle exit plane. In addition to revealing the nature of the flow, the inviscid solution provides the upper limit of the pressures achieved on the ground and fuselage. The inviscid solution is also the zeroth order configuration which is needed to compute viscous entrainment by the flow.

SYMBOLS

A a constant

A_o a constant

C_p pressure coefficient

H	quantity defined in eq. (A8)
I	flow region in φ-plane
J	flow region in W-plane
K	complete elliptic integral of first kind
K'	defined by $K'(k) \equiv K(k')$
k	modulus of elliptic integral
k'	defined as $\sqrt{1 - k^2}$
M	quantity defined in eq. (18)
p	pressure
p_o	ambient pressure outside jets
Q	functions defined in eqs. (B4) and (B5) of ref. 3
R	functions defined in eqs. (B2) and (B3) of ref. 3
T	complex variable in T-plane, $\xi + i\eta$
t	complex variable in t-plane
u	velocity in x-direction
V	velocity
V_I	velocity at nozzle exit
$\overline{V}_I$	average velocity at nozzle exit
V_o	velocity along free streamlines
v	velocity in y-direction
W	complex potential, $\Phi + i\psi$
X_N, Y_N	coordinates of center of nozzle exit plane nondimensionalized by Δ
x, y	coordinates in physical plane
z	complex variable, $x + iy$
β	tilt angle of plate, fig. 3
Γ	flow region in T-plane
γ	angle of deflected jet, fig. 3
Δ	width of nozzle
δ_L, δ_R	widths of streams flowing to left and to right

ζ	complex conjugate velocity, u - iv
ρ	density
ξ, η	coordinates of T-plane
Θ	quantity defined in eq. (A7)
Φ	velocity potential
ψ	stream function
Ω	function defined in appendix A of ref. 3

Subscripts:

A,G,H	refer to stagnation points, fig. 3
f	fuselage
g	ground
L	flow to left
R	flow to right

ANALYSIS

The analysis presented herein is a generalization of, and quite similar to, that given in reference 3. For this reason only those parts of the analysis differing from reference 3 will be discussed in detail. The configuration of the flow, as shown in figure 2, is symmetric about a vertical plane between the nozzles, hence only half the flow field need be considered. The boundaries of the jet in the physical plane (z-plane) are shown in figure 3. Since the region outside the jet is at constant pressure, Bernoulli's equation shows that the velocity has constant magnitude along the free streamlines $\widehat{DE}$, $\widehat{CF}$, and $\widehat{BF}$. The direction of the velocity must be along the boundaries on $\widehat{AB}$, $\widehat{AG}$, and $\widehat{GHE}$ corresponding respectively to the bottom of the fuselage, the vertical line of symmetry, and the ground. The point H is a stagnation point at which the direction of the velocity along $\widehat{GHE}$ must reverse. The dashed line is the dividing streamline of the flows going to the right and left. The points G and A are also stagnation points. Along the line $\widehat{CD}$ the velocity is vertically downward.

As in reference 3, let ζ be the complex conjugate velocity u - iv. From the specified conditions on the velocity at the boundaries of the flow field, it can be deduced that the flow field in figure 3 maps into the interior of the region I of the hodograph plane

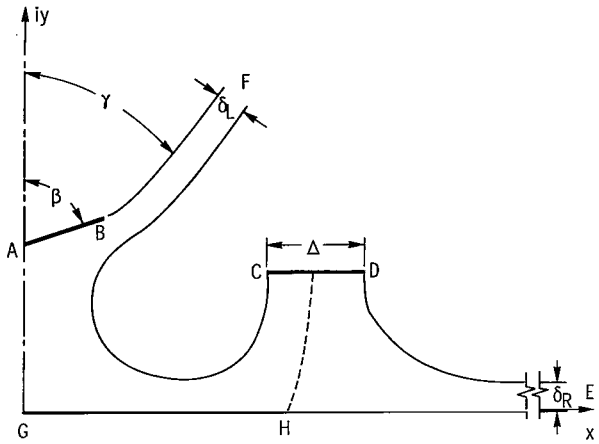

Figure 3. - Flow boundaries in physical z-plane (z = x + iy).

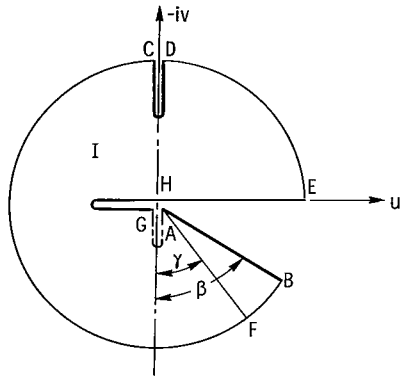

Figure 4. - Flow region in hodograph ζ-plane (ζ = u - iv).

shown in figure 4. Let $W = \Phi + i\psi$ be the complex potential for the flow, where Φ is the velocity potential and ψ is the stream function. Considerations analogous to those in reference 3 show that the flow field maps into the interior of the region J of the complex potential plane in figure 5.

The solution in the physical plane is obtained from the integration

$$z = \int \frac{1}{\zeta} dW + \text{constant} \tag{1}$$

To carry out this integral, ζ and W must be expressed in terms of the same variable of integration. This is done by appropriately mapping the rectangular region Γ of an intermediate T-plane (described in ref. 3 and depicted in fig. 7) into the regions I and J of the ζ and W planes, respectively. The corresponding positions of the boundaries of Γ, I, and J are indicated by the lettering scheme in figures 4, 5, and 7.

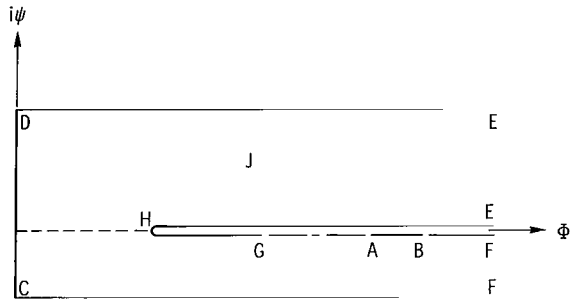

Figure 5. - Complex potential plane (W = Φ + iψ).

Mapping Function Between ζ and T-Planes

The function ζ which properly maps the rectangle Γ into the region I of the ζ-plane can be constructed by using the function Ω defined and studied in appendix A of reference 3. By a procedure completely analogous to that in reference 3, it can be demonstrated that the proper mapping function ζ is given by

$$\zeta(T) = V_o e^{i(\pi/2)} \Omega(T; \xi_H, k) \sqrt{\Omega(T; \xi_G, k)} \left[\Omega(T; \xi_A, k)\right]^{\beta/\pi}; \quad T \in \Gamma \tag{2}$$

provided that the relation between ξ_H, ξ_G, and ξ_A is chosen to satisfy the following requirement. Along the plate $\widehat{AB}$ the argument of $\zeta(T)$ must equal the direction along the plate, so that from figure 4

$$\arg \zeta(T) = \frac{3\pi}{2} + \beta; \quad T \in \widehat{AB}$$

It follows by the use of equation (A24) of appendix A of reference 3 that the argument of equation (2) is

$$\arg \zeta(T) = \frac{\pi}{2} + \frac{\pi}{2}\left(\frac{\xi_H}{K} + 1\right) + \frac{\pi}{4}\left(\frac{\xi_G}{K} + 1\right) + \frac{\beta}{2}\left(\frac{\xi_A}{K} + 1\right); \quad T \in \widehat{AB}$$

Equating the previous two expressions for $\arg \zeta(T)$ gives the condition relating ξ_H, ξ_G, and ξ_A:

$$\left(\frac{\pi}{4} + \frac{\beta}{2}\right)\frac{4K}{\pi} = 2\xi_H + \xi_G + \frac{2\beta}{\pi}\xi_A \tag{3}$$

Mapping Function Between W and T Planes

The function W which properly maps the rectangle Γ of the T-plane (fig. 7) into the region J of the W-plane (fig. 5) can be constructed by use of the intermediate t-plane shown in figure 6. An application of the Schwarz-Christoffel transformation shows that the mapping that transforms the upper half t-plane onto the region J of the W-plane in the manner indicated in figures 5 and 6 is defined by

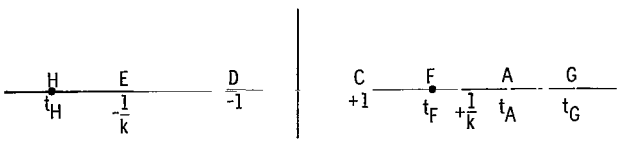

Figure 6. - Intermediate t-plane.

$$\frac{dW}{dt} = iA_o \frac{t - t_H}{(1 + kt)(t_F - t)\sqrt{1 - t^2}}; \quad \mathcal{I}m\, t > 0 \tag{4}$$

Now it is shown in reference 3 that the rectangle Γ of the T-plane is mapped onto the upper half t-plane (fig. 6) by

$$t = sn(T, k); \quad T \in \Gamma \tag{5}$$

This can be combined with equation (4) to eliminate t and find the desired mapping from the T-plane to the W-plane. The relation given in reference 3 is used

$$t_H = \frac{1}{k\, sn(\xi_H, k)}$$

along with the relation

$$t_F = sn(T_F, k) = sn(K + i\eta_F, k) = \frac{cn(i\eta_F, k)}{dn(i\eta_F, k)} = \frac{1}{cn(\eta_F, k')} \frac{cn(\eta_F, k')}{dn(\eta_F, k')} = \frac{1}{dn(\eta_F, k')}$$

Upon carrying out this procedure the required function that maps Γ onto J is found to be

$$\frac{dW}{dT} = iA \frac{(k\, sn\xi_H snT - 1)\, dnT}{(1 + k\, snT)\left[1 - dn(\eta_F, k')snT\right]}; \quad T \in \Gamma \tag{6}$$

where A is a new constant equal to

$$A_o \frac{dn(\eta_F, k')}{k\, sn\xi_H}$$

By using partial fractions equation (6) can be rewritten as

$$\frac{dW}{d(snT)} = \frac{iA}{k + dn(\eta_F, k')} \left\{ \frac{k\, sn\xi_H - dn(\eta_F, k')}{\sqrt{1 - sn^2T}\left[1 - dn(\eta_F, k')snT\right]} - \frac{k(1 + sn\,\xi_H)}{\sqrt{1 - sn^2T}\,(1 + k\, snT)} \right\}$$

Integrating this expression and neglecting an unimportant integration constant give

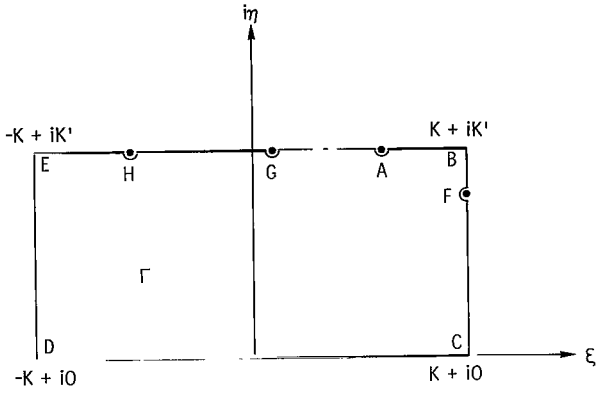

Figure 7. - Mapping of jet flow into region Γ of T-plane (T = ξ + iη).

(7)

The flow through the nozzle is equal to the difference between the stream function at points D and C. Noting that $W = \Phi + i\psi$ and that $\Phi(C) = \Phi(D)$, the flow must equal $\psi(D) - \psi(C) = \left[W(D) - W(C)\right]/i$. When the coordinates of D and C in figure 7 are used, the flow through the nozzle becomes: $\left[W(-K + i0) - W(K + i0)\right]/i$. Hence, if $\overline{V}_I$ is the average velocity at the nozzle exit,

$$\overline{V}_I\, \Delta = \frac{W(-K + i0) - W(K + i0)}{i}$$

$$W = \frac{iA}{k + dn(\eta_F, k')} \left\{ \left[k\, sn\xi_H - dn(\eta_F, k')\right] \int^{snT} \frac{dt}{\sqrt{1 - t^2}\left[1 - dn(\eta_F, k')t\right]} - k(1 + sn\,\xi_H) \int^{snT} \frac{dt}{\sqrt{1 - t^2}(1 + kt)} \right\}$$

$$= \frac{iA}{k'sn(\eta_F, k')\left[k + dn(\eta_F, k')\right]} \left\{ \left[dn(\eta_F, k') - k\, sn\xi_H\right] \sin^{-1}\left[\frac{dn(\eta_F, k') - snT}{dn(\eta_F, k')snT - 1}\right] - k(1 + sn\,\xi_H)sn(\eta_F, k') \sin^{-1}\left[\frac{k + snT}{1 + k\, snT}\right] \right\}$$

Using the fact that $sn(\pm K) = \pm 1$ and choosing the appropriate branches for the inverse sine, we find from equation (7)

$$W(K) = \frac{iA}{k' sn(\eta_F, k')\left[k + dn(\eta_F, k')\right]} \left\{\left[dn(\eta_F, k') - k\, sn\xi_H\right] \frac{\pi}{2} - k(1 + sn\xi_H) sn(\eta_F, k') \frac{\pi}{2}\right\}$$

$$W(-K) = \frac{iA}{k' sn(\eta_F, k')\left[k + dn(\eta_F, k')\right]} \left\{\left[dn(\eta_F, k') - k\, sn\xi_H\right] \frac{3\pi}{2} - k(1 + sn\xi_H) sn(\eta_F, k') \left(-\frac{\pi}{2}\right)\right\}$$

Hence,

$$\overline{V}_I \Delta = \frac{A\pi}{k' sn(\eta_F, k')\left[k + dn(\eta_F, k')\right]} \left[dn(\eta_F, k') - k\, sn\xi_H + k(1 + sn\xi_H) sn(\eta_F, k')\right]$$

which gives the constant A as

$$A = \frac{\overline{V}_I \Delta}{\pi} k' sn(\eta_F, k') \left\{1 + (1 + sn\xi_H) k \left[\frac{sn(\eta_F, k') - 1}{dn(\eta_F, k') + k}\right]\right\}^{-1} \tag{8}$$

An alternate form for A will be given by equation (15).

As shown in figure 3, the interaction of the jet with the ground causes it to divide. The asymptotic width of the flow region to the right is designated by δ_R, and that to the left by δ_L. The flow to the left must equal the jump in the imaginary part of W at the point F. In order to evaluate this jump, notice that F is at $T = K + i\eta_F$ along the boundary $T = K + i\eta$ in figure 7 and that

$$sn(K + i\eta) = \frac{1}{dn(\eta, k')}$$

Then, along this boundary, the inverse sine terms in W (eq. (7)) become

$$\sin^{-1}\left[\frac{dn(\eta_F, k') - \dfrac{1}{dn(\eta, k')}}{\dfrac{dn(\eta_F, k')}{dn(\eta, k')} - 1}\right]$$

$$= -i \ln\left(i\left\{\frac{1 - dn(\eta_F, k')\, dn(\eta, k') + \sqrt{\left[1 - dn^2(\eta, k')\right]\left[1 - dn^2(\eta_F, k')\right]}}{dn(\eta, k') - dn(\eta_F, k')}\right\}\right)$$

$$= \frac{\pi}{2} - i \ln\left[f_1(\eta)\right] + i \ln\left[dn(\eta, k') - dn(\eta_F, k')\right]$$

where

$$f_1(\eta) = 1 - dn(\eta_F, k')\, dn(\eta, k') + \sqrt{\left[1 - dn^2(\eta, k')\right]\left[1 - dn^2(\eta_F, k')\right]}$$

$$\sin^{-1}\left[\frac{k + \dfrac{1}{dn(\eta, k')}}{1 + \dfrac{k}{dn(\eta, k')}}\right] = -i \ln\left\{i\left[\frac{k\, dn(\eta, k') + 1}{dn(\eta, k') + k}\right] + k' \frac{\sqrt{dn^2(\eta, k') - 1}}{dn(\eta, k') + k}\right\}$$

$$= \frac{\pi}{2} - i \ln\left[f_2(\eta)\right]$$

where

$$f_2(\eta) = \frac{k\, dn(\eta, k') + k'^2 sn(\eta, k') + 1}{k + dn(\eta, k')}$$

Since $0 < dn(\eta, k') \leq 1$ and $sn(\eta, k')$ is positive for $0 \leq \eta \leq K'$ it is found that $f_1(\eta) > 0$ and $f_2(\eta) > 0$ for $0 \leq \eta \leq K'$ and, consequently, the logarithms of f_1 and f_2 are real.

Hence, choosing the appropriate branch for the $\ln\left[dn(\eta, k') - dn(\eta_F, k')\right]$ term and substituting in equation (7) gives

$$\mathcal{I}m\, W(K + i\eta) = \frac{A\pi}{k' sn(\eta_F, k')\left[k + dn(\eta_F, k')\right]} \left\{\frac{1}{2}\left[dn(\eta_F, k') - k\, sn\xi_H\right]\right.$$

$$\left. - \frac{k}{2}(1 + sn\,\xi_H) sn(\eta_F, k')\right\}; \qquad \eta > \eta_F \qquad (9)$$

$$\mathcal{I}m\, W(K + i\eta) = \frac{A\pi}{k' sn(\eta_F, k')\left[k + dn(\eta_F, k')\right]} \left\{-\frac{1}{2}\left[dn(\eta_F, k') - k\, sn\xi_H\right]\right.$$

$$\left. - \frac{k}{2}(1 + sn\,\xi_H) sn(\eta_F, k')\right\}; \qquad \eta < \eta_F \qquad (10)$$

Since the velocity at the point F must be V_o, it follows from equations (9) and (10) that, if δ_L is the asymptotic perpendicular jet width (fig. 3) and $\epsilon > 0$,

$$\delta_L V_o = \lim_{\epsilon \to 0} \mathcal{I}m\left\{W\left[K + i(\eta_F + \epsilon)\right] - W\left[K + i(\eta_F - \epsilon)\right]\right\}$$

$$= \frac{A\pi}{k' sn(\eta_F, k')\left[k + dn(\eta_F, k')\right]}\left[dn(\eta_F, k') - k\, sn\xi_H\right]$$

$$= \frac{A\pi}{k' sn(\eta_F, k')}\left[1 - \frac{k(1 + sn\,\xi_H)}{k + dn(\eta_F, k')}\right]$$

Equation (8) is used to eliminate A giving

$$\delta_L V_o = \overline{V}_I\, \Delta \frac{k + dn(\eta_F, k') - k(1 + sn\,\xi_H)}{k + dn(\eta_F, k') - k(1 + sn\,\xi_H)\left[1 - sn(\eta_F, k')\right]} \qquad (11)$$

Continuity requirements dictate that

$$\delta_R V_o + \delta_L V_o = \Delta \overline{V}_I$$

Hence, using equation (11), the δ_L can be eliminated to obtain

$$\frac{\delta_R}{\Delta} = \frac{\overline{V}_I}{V_o} \frac{k(1 + sn\,\xi_H) sn(\eta_F, k')}{k + dn(\eta_F, k') - k(1 + sn\,\xi_H)\left[1 - sn(\eta_F, k')\right]} \qquad (12)$$

From equations (12) and (11) the ratio of asymptotic widths is

$$\frac{\delta_R}{\delta_L} = \frac{\mathrm{sn}(\eta_F, k')}{\dfrac{k + \mathrm{dn}(\eta_F, k')}{k(1 + \mathrm{sn}\,\xi_H)} - 1}$$

By rearrangement

$$\frac{k(1 + \mathrm{sn}\,\xi_H)}{k + \mathrm{dn}(\eta_F, k')} = \frac{1}{\dfrac{\delta_L}{\delta_R}\,\mathrm{sn}(\eta_F, k') + 1} \tag{13}$$

and

$$\mathrm{sn}\,\xi_H = \frac{\dfrac{\delta_R}{\delta_L}\,\mathrm{dn}(\eta_F, k') - k\,\mathrm{sn}(\eta_F, k')}{\dfrac{\delta_R}{\delta_L}\,k + k\,\mathrm{sn}(\eta_F, k')} \tag{14}$$

Using equation (14) in equation (8) gives the constant A as

$$A = \frac{\overline{V}_I\,\Delta}{\pi}\,k'\left[\frac{\mathrm{sn}(\eta_F, k') + \dfrac{\delta_R}{\delta_L}}{1 + \dfrac{\delta_R}{\delta_L}}\right] \tag{15}$$

Integration to Yield Coordinates in Physical Plane

When the complex conjugate velocity ζ and the complex potential W as functions of the parametric variable T are known, the physical variable z can be found as a function of T by using equation (1). The integration is carried out in the T-plane instead of in the W-plane, so that equation (1) becomes

$$z = \int_{\xi_G + iK'}^{T} \frac{1}{\zeta(T)} \frac{dW}{dT} dT \tag{16}$$

The origin of the coordinate system has been chosen at the point G. Substituting equations (2), (6), and (15) in equation (16) gives

$$\frac{z}{\Delta} = \left(\frac{\overline{V}_I}{V_o}\right) \frac{k'}{\pi} \left[\frac{sn(\eta_F, k') + \frac{\delta_R}{\delta_L}}{1 + \frac{\delta_R}{\delta_L}}\right]$$

$$\times \int_{\xi_G + iK'}^{T} \frac{(k\, sn\xi_H snT - 1)(1 - k\, snT)\, dT}{dnT\left[1 - dn(\eta_F, k')snT\right]\Omega(T; \xi_H, k)\sqrt{\Omega(T; \xi_G, k)}\left[\Omega(T; \xi_A, k)\right]^{\beta/\pi}} \tag{17}$$

Average Velocity at Nozzle Exit

To find an expression for $\overline{V}_I/V_o$, note that the nozzle width is given by

$$\Delta = z(-K + i0) - z(K + i0)$$

Then it follows from equation (17)

$$\frac{\overline{V}_I}{V_o}\left[\frac{sn(\eta_F, k') + \frac{\delta_R}{\delta_L}}{1 + \frac{\delta_R}{\delta_L}}\right] \equiv M = \left\{\frac{k'}{\pi} \int_{-K}^{K} \frac{(1 - k\, sn\xi_H sn\xi)(1 - k\, sn\xi)\, d\xi}{dn\xi\left[1 - dn(\eta_F, k')sn\xi\right]\Omega(\xi; \xi_H, k)\sqrt{\Omega(\xi; \xi_G, k)}\left[\Omega(\xi; \xi_A, k)\right]^{\beta/\pi}}\right\}^{-1} \tag{18}$$

The quantity M defined in this equation will be used subsequently.

Pressure Coefficients

The pressure coefficients $C_{p,g}$ and $C_{p,f}$ along the ground and fuselage are defined by

$$C_{p,g} = \frac{p(x, 0) - p_o}{\frac{1}{2}\rho V_o^2}$$

$$C_{p,f} = \frac{p(x_f, y_f) - p_o}{\frac{1}{2}\rho V_o^2}$$

where x_f, y_f are the coordinates of the points along the fuselage. Using Bernoulli's equation gives

$$C_{p,g} = 1 - \left[\frac{u(\xi, K')}{V_o}\right]^2; \qquad -K \le \xi \le \xi_G \tag{19}$$

$$C_{p,f} = 1 - \left[\frac{u^2(\xi, K') + v^2(\xi, K')}{V_o^2}\right]; \qquad \xi_A \le \xi \le K \tag{20}$$

Summary of Analytical Relations

For convenience, the results of this section are now collected in one place.

$$\operatorname{sn}\xi_H = \frac{\frac{\delta_R}{\delta_L}\operatorname{dn}(\eta_F, k') - k\operatorname{sn}(\eta_F, k')}{\frac{\delta_R}{\delta_L}k + k\operatorname{sn}(\eta_F, k')} \tag{14}$$

$$\left(\frac{\pi}{4} + \frac{\beta}{2}\right)\frac{4K}{\pi} = 2\xi_H + \xi_G + \frac{2\beta}{\pi}\xi_A \tag{3}$$

$$\frac{\zeta(T)}{V_o} = i\Omega(T; \xi_H, k)\sqrt{\Omega(T; \xi_G, k)}\left[\Omega(T; \xi_A, k)\right]^{\beta/\pi} \tag{2}$$

$$\frac{W(T)}{\overline{V}_I \Delta} = \frac{i}{\pi} \frac{1}{\left[dn(\eta_F, k') + k\right] + (1 + sn\xi_H)k\left[sn(\eta_F, k') - 1\right]}$$

$$\times \left\{ \left[dn(\eta_F, k') - k\, sn\xi_H \right] \sin^{-1} \left[\frac{dn(\eta_F, k') - snT}{dn(\eta_F, k')snT - 1} \right] \right.$$

$$\left. - k(1 + sn\xi_H)sn(\eta_F, k') \sin^{-1} \left[\frac{k + snT}{1 + k\, snT} \right] \right\} \qquad (7, 8)$$

$$\frac{z(T)}{\Delta} = \left(\frac{\overline{V}_I}{V_o} \right) \frac{k'}{\pi} \left[\frac{sn(\eta_F, k') + \frac{\delta_R}{\delta_L}}{1 + \frac{\delta_R}{\delta_L}} \right]$$

$$\times \int_{\xi_G + iK'}^{T} \frac{(k\, sn\xi_H snT - 1)(1 - k\, snT)\, dT}{dnT\left[1 - dn(\eta_F, k')snT\right] \Omega(T; \xi_H, k) \sqrt{\Omega(T; \xi_G, k)} \left[\Omega(T; \xi_A, k)\right]^{\beta/\pi}} \qquad (17)$$

$$\frac{\delta_R}{\Delta} = \frac{\overline{V}_I}{V_o} \frac{k(1 + sn\xi_H)sn(\eta_F, k')}{k + dn(\eta_F, k') - k(1 + sn\xi_H)\left[1 - sn(\eta_F, k')\right]} \qquad (12)$$

$$\frac{\overline{V}_I}{V_o} \left[\frac{sn(\eta_F, k') + \frac{\delta_R}{\delta_L}}{1 + \frac{\delta_R}{\delta_L}} \right] \equiv M = \left\{ \frac{k'}{\pi} \int_{-K}^{K} \frac{(1 - k\, sn\xi_H sn\xi)(1 - k\, sn\xi)\, d\xi}{dn\xi \left[1 - dn(\eta_F, k')sn\xi\right] \Omega(\xi; \xi_H, k) \sqrt{\Omega(\xi; \xi_G, k)} \left[\Omega(\xi; \xi_A, k)\right]^{\beta/\pi}} \right\}^{-1} \qquad (18)$$

$$C_{p,g} = 1 - \left[\frac{u(\xi, K')}{V_o} \right]^2; \qquad -K \le \xi \le \xi_G \qquad (19)$$

$$C_{p,f} = 1 - \left[\frac{u^2(\xi, K') + v^2(\xi, K')}{V_o^2} \right]; \qquad \xi_A \le \xi \le K \qquad (20)$$

Additional forms of equations (2) and (17) that are useful for computer evaluation are given in the appendix.

COMPUTATIONAL PROCEDURE

If all coordinates are nondimensionalized by the nozzle width Δ, there are five independent parameters governing the flow configuration: plate (fuselage) height above the ground, plate width, plate angle, nozzle height, and spacing between nozzles. The plate angle β appears explicitly in the analytical expressions and can be directly specified as an input variable in the computer program used to evaluate numerical results. The other four physical quantities must be found by computation in terms of four convenient input quantities all having values between 0 and 1: k, δ_L/δ_R, η_F/K', and ξ_A/K. From a chosen k, the k', K, and K' can be found from

$$k' = \sqrt{1 - k^2}$$

$$K(k) = \int_0^{\pi/2} \frac{dw}{\sqrt{1 - k^2 \sin^2 w}}$$

$$K'(k) = K(k')$$

Then ξ_H can be found from equation (14), and all quantities which are necessary to determine ξ_G from equation (3) will then be known. The quantities M and $\overline{V}_I/V_o$ are then found by carrying out the integration in equation (18), using the Ω functions evaluated by the method described in the appendixes of reference 3. The dimensionless width of the stream flowing to the right δ_R/Δ is evaluated from equation (12), and δ_L/Δ is computed from $(\delta_R/\Delta)(\delta_L/\delta_R)$, where δ_L/δ_R is one of the specified input quantities.

With all these quantities evaluated, the height of the plate is found from equation (A6), and its width by integrating equation (A5) to an upper limit of K. These dimensions, along with the specified angle β, fix the position of point B. The streamline $\overset{\frown}{BF}$ can then be plotted by use of equation (A12). The distance in equation (A10) is then evaluated to fix the horizontal position of the nozzle. The vertical separation of points D and E along the right free streamline is found from the second of equations (A9) by integrating to an upper limit of K'. This distance, along with δ_R/Δ, is used to determine the nozzle height. The free streamlines originating at the nozzle are then computed from equations (A9) and (A11) and are drawn starting, respectively, from points D and C.

The pressure coefficients along the ground and fuselage are found from equations (19) and (20) using the velocities evaluated from the second equations of (A4) and (A5).

RESULTS AND DISCUSSION

As revealed by the analysis, there are several independent parameters (all made dimensionless by dividing by the nozzle width) governing the flow: the nozzle height, spacing between nozzles, plate height, plate width, and plate angle. It was not feasible to systematically compute flow patterns for the wide variety of possible combinations of these parameters. To limit the number of computed flow patterns somewhat, the plate simulating the underside of the fuselage was fixed in a horizontal orientation with the exception of the results shown in figure 12 where a comparison is made with a plate tilted at 45^{o}. The plate was generally positioned at the same height as the nozzle, and only two nozzle heights were considered (Y_N = 1 and 2).

Consider figure 8(a) as a typical set of results. On each set two cases are given, one in solid lines and the other dashed. Each case shows the velocity distribution across the nozzle exit plane, the free streamlines bounding the moving fluid, the pressure coefficient along the ground, and the pressure coefficient along the plate (fuselage).

Figures 8(a) and (b) illustrate the effect of moving the nozzle and plate upward together, as when the airplane is taking off. Part (b) is for a longer plate than part (a), but both portions of the figure exhibit the same general features. In the upper position the exit velocity from the nozzle is more uniform; hence, the flow is increased as the nozzle is raised since there is less reaction from the ground. The increase in flow results in the integral of the ground pressure coefficient being a little larger for the upper nozzle position, thus providing a small increase in lift. The pressure coefficient acting on the underside of the plate is decreased a little as the plate and nozzle are raised, thereby reducing the lift on the fuselage. In figure 8(b) the stream deflection by the plate is so large for the upper nozzle position (dashed) that the stream passes back into the region of the nozzle exit. In an actual flow the two streams would collide. The analysis used herein does not allow for such interference and permits the two streams to pass independently through each other (on different sheets of the complex plane). Actually, there would be interference and probably a recirculating flow region for this configuration.

Figure 9 demonstrates the effect of changing the horizontal position of the nozzle. Parts (a) and (b) are for a low nozzle (Y_N = 1), while parts (c) and (d) are for a high nozzle (Y_N = 2). The dominant effect is that the flow going to the left and impinging under the fuselage becomes quite small as the nozzles approach the plate. Thus having the fan pod adjacent to the fuselage rather than as shown in figure 1(a) will reduce the hot gas circulation around the fuselage. Recall that this is a two-dimensional analysis. If the nozzles were round rather than in a slot or pod configuration, there would be an additional effect of nozzle spacing resulting from the radial spreading of the flow as it moves outward along the ground. This effect along with entrainment would tend to decrease the flow under the fuselage as the spacing between nozzles is increased.

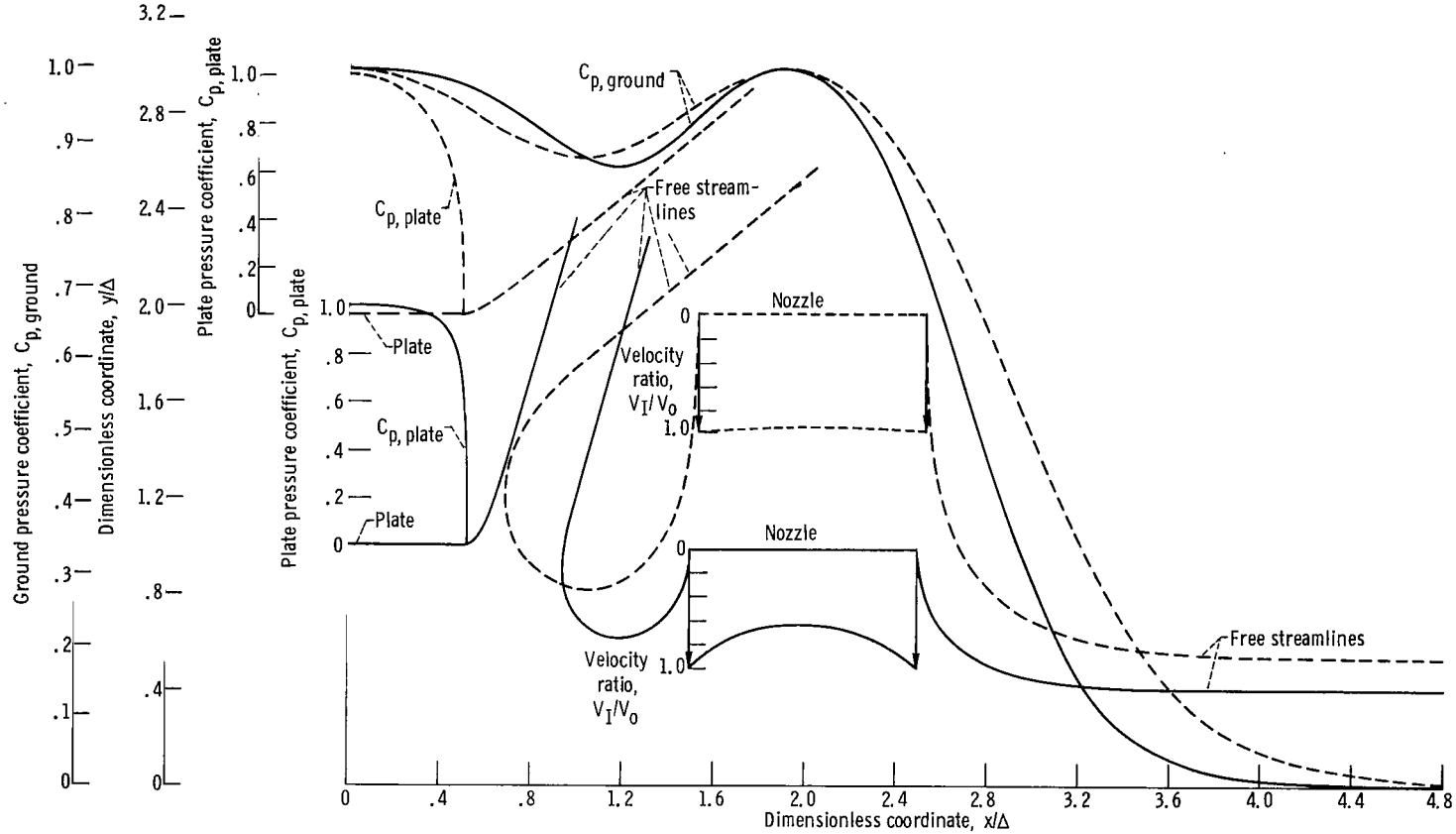

(a) Plate width ≈0.5.

Figure 8. - Effect of vertical position of both nozzle and plate.

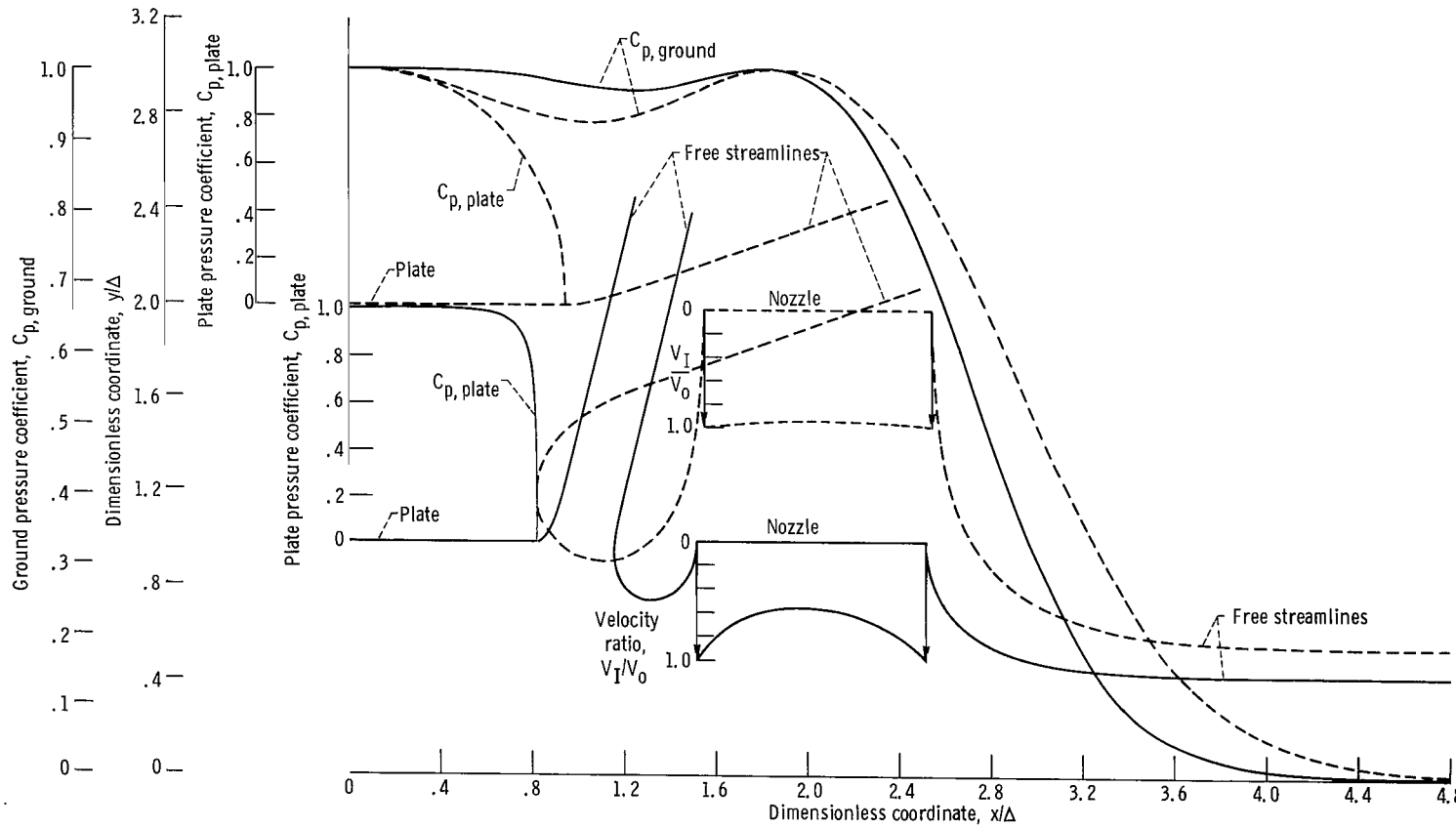

(b) Plate width ≈0.9.

Figure 8. - Concluded.

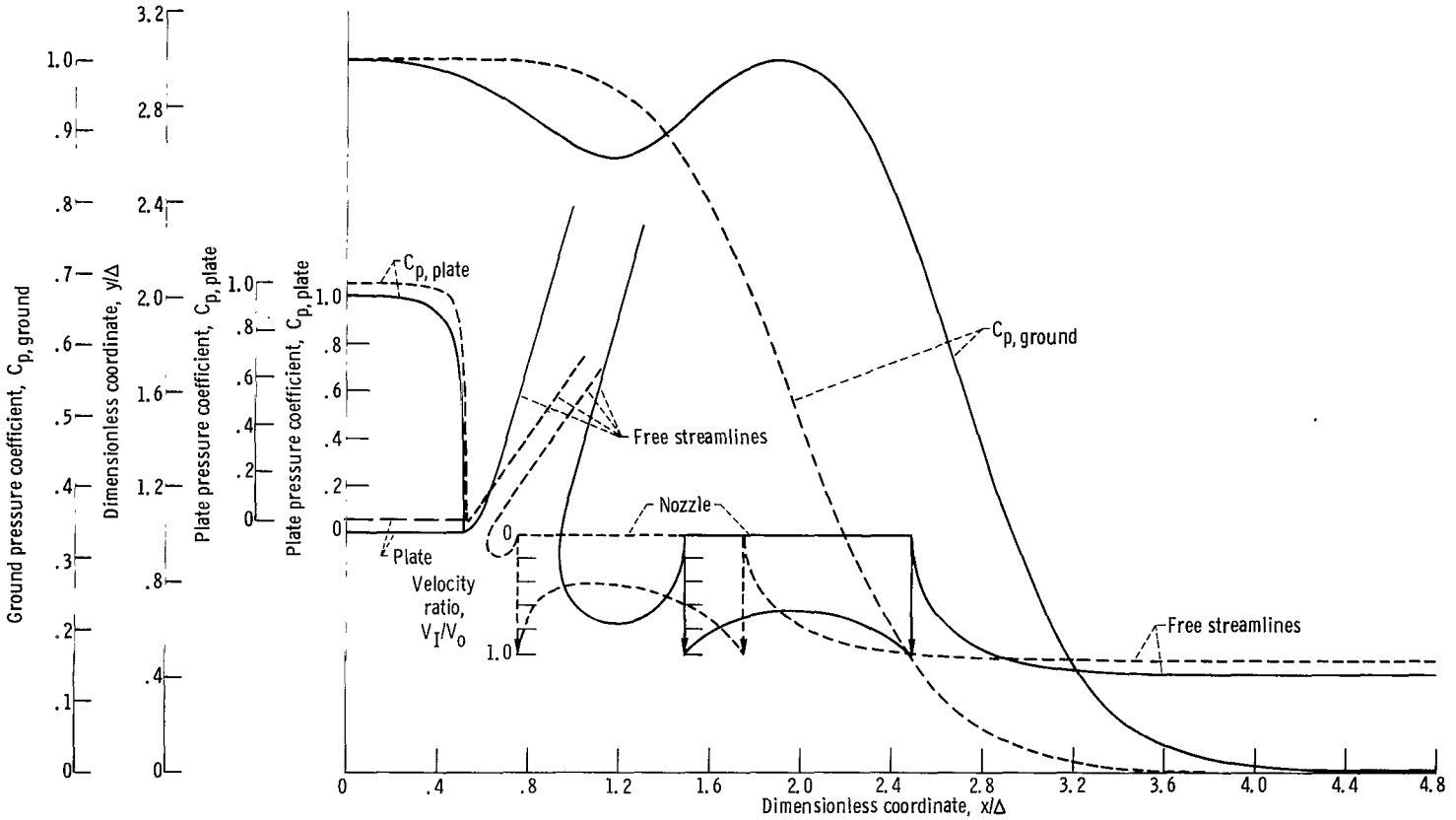

(a) Low nozzle (Y_N = 1); plate width ≈0.5.

Figure 9. - Effect of horizontal position of nozzle.

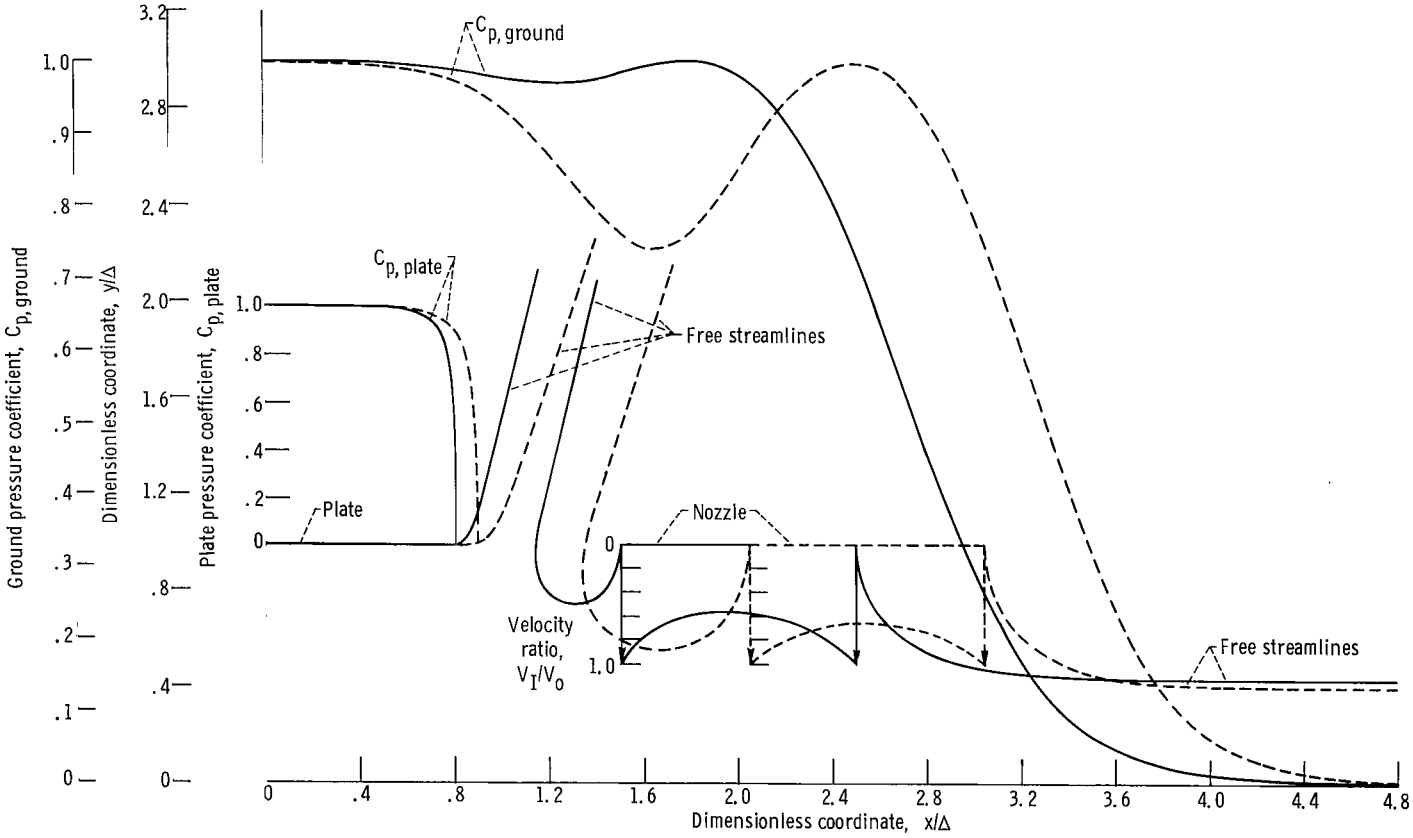

(b) Low nozzle (Y_N = 1); plate width ≈0.8.

Figure 9. - Continued.

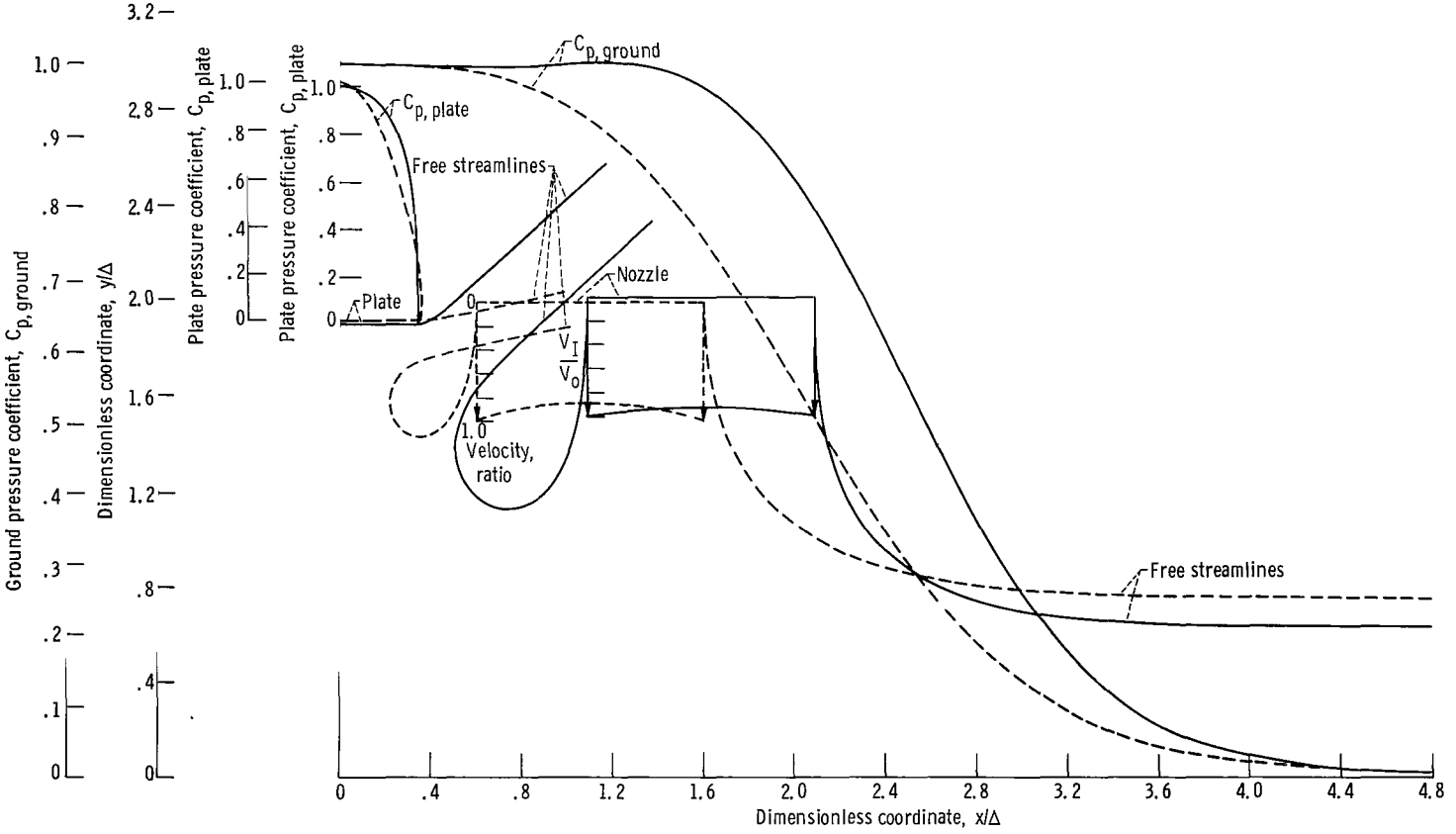

(c) High nozzle (Y_N = 2); plate width ≈0.4.

Figure 9. - Continued.

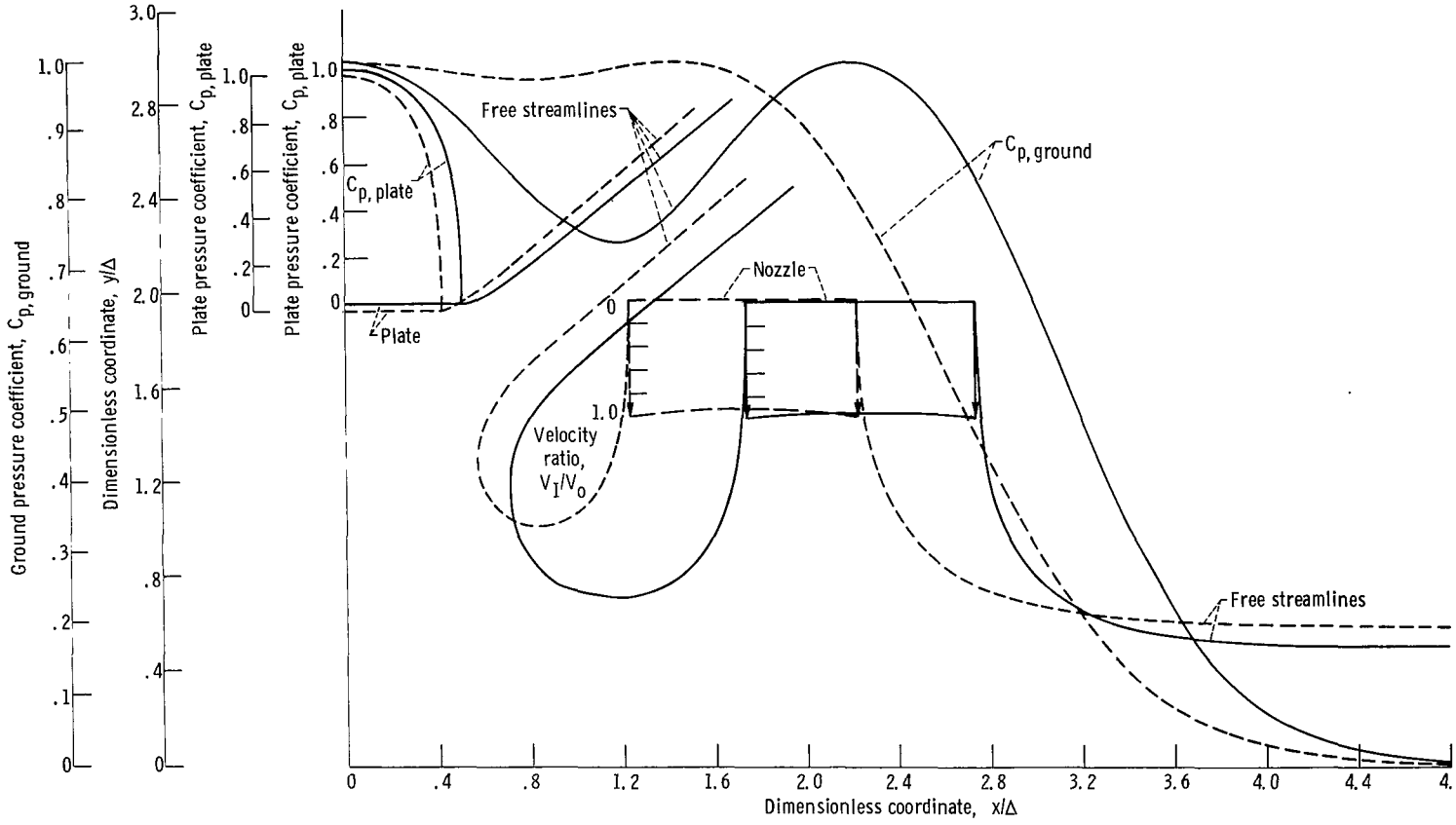

(d) High nozzle (Y_N = 2); plate width ≈0.5.

Figure 9. - Concluded.

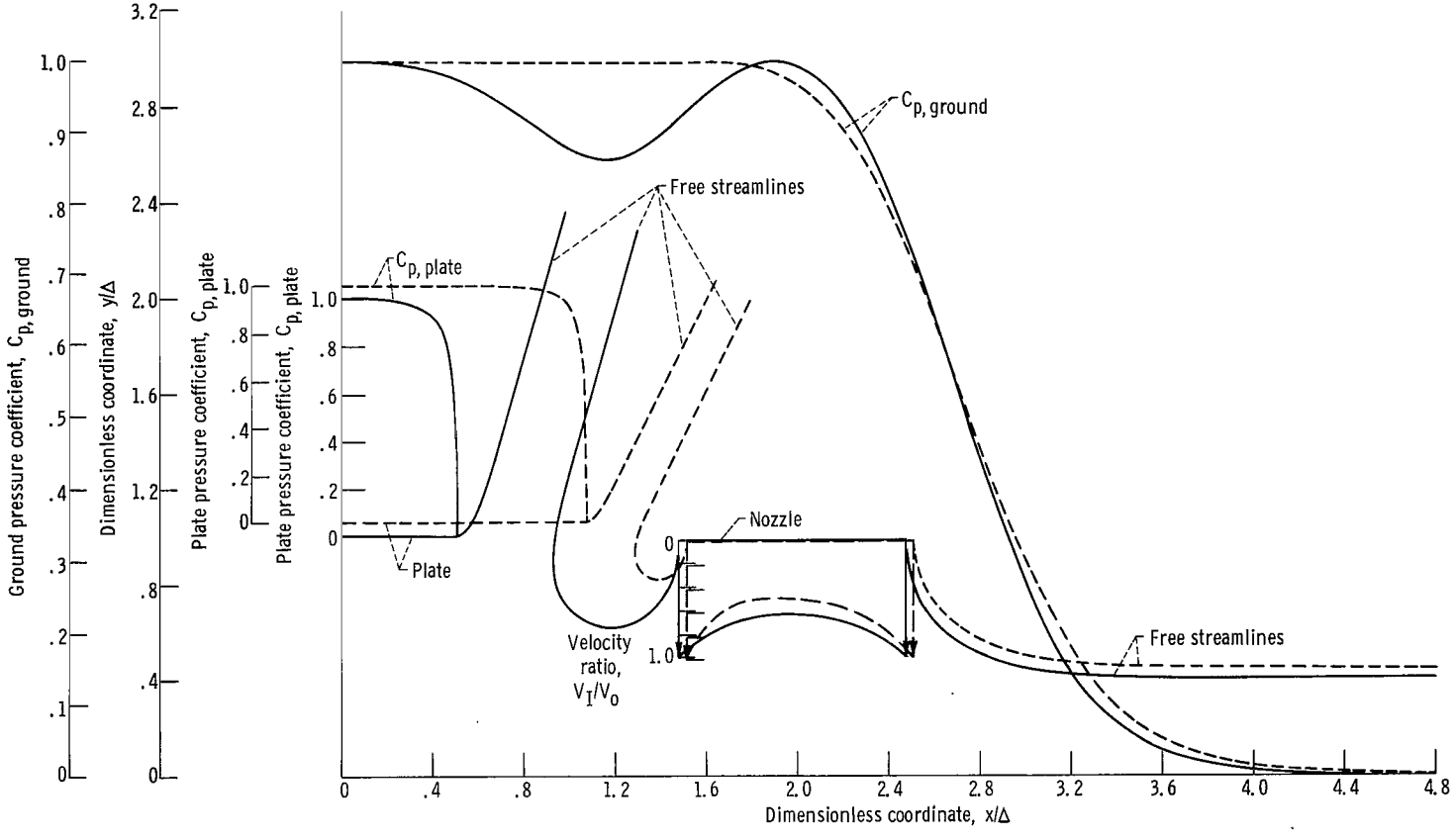

(a) Low nozzle (Y_N = 1).

Figure 10. - Effect of plate width for fixed nozzle position.

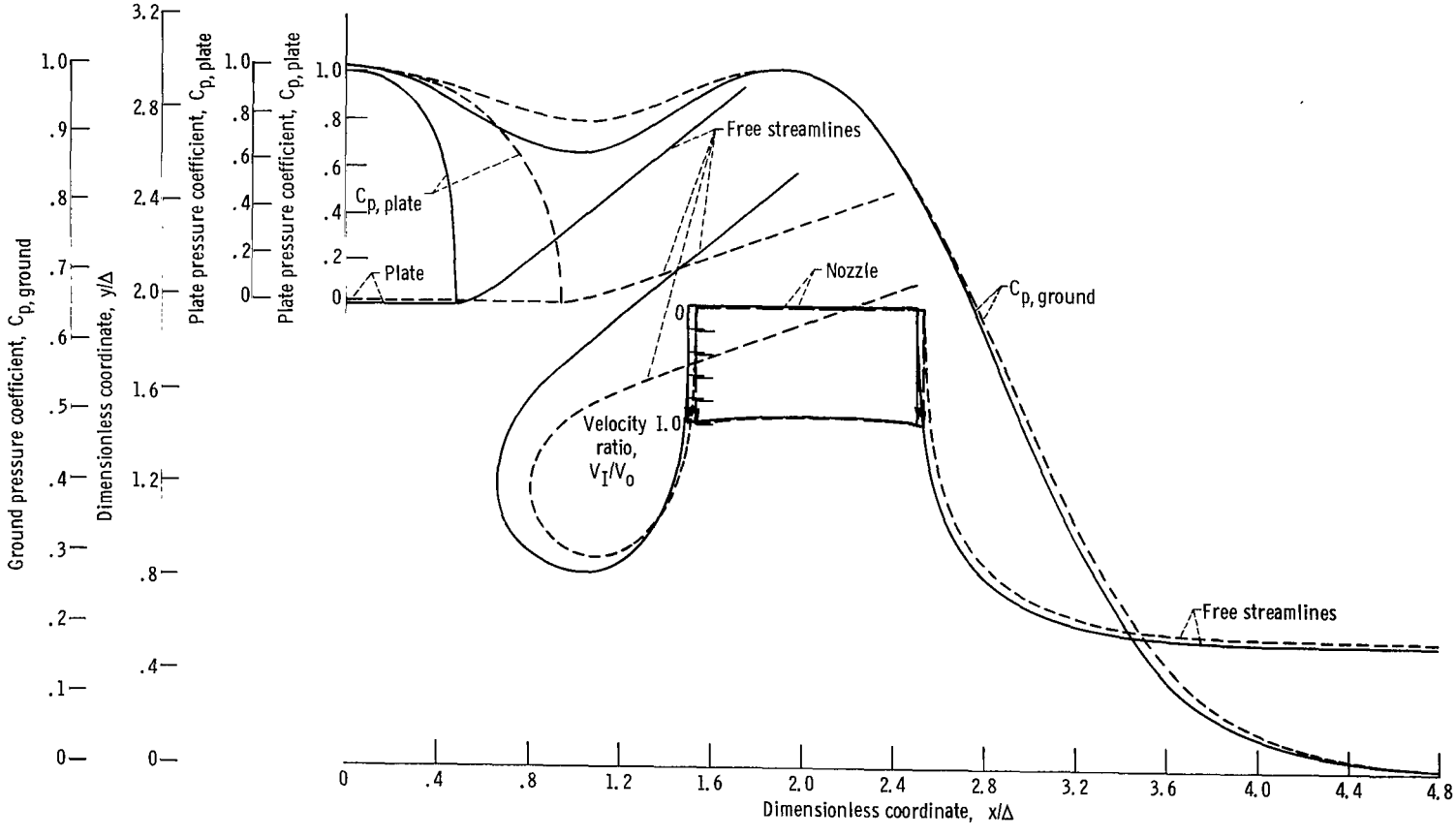

(b) High nozzle (Y_N = 2).

Figure 10. - Concluded.

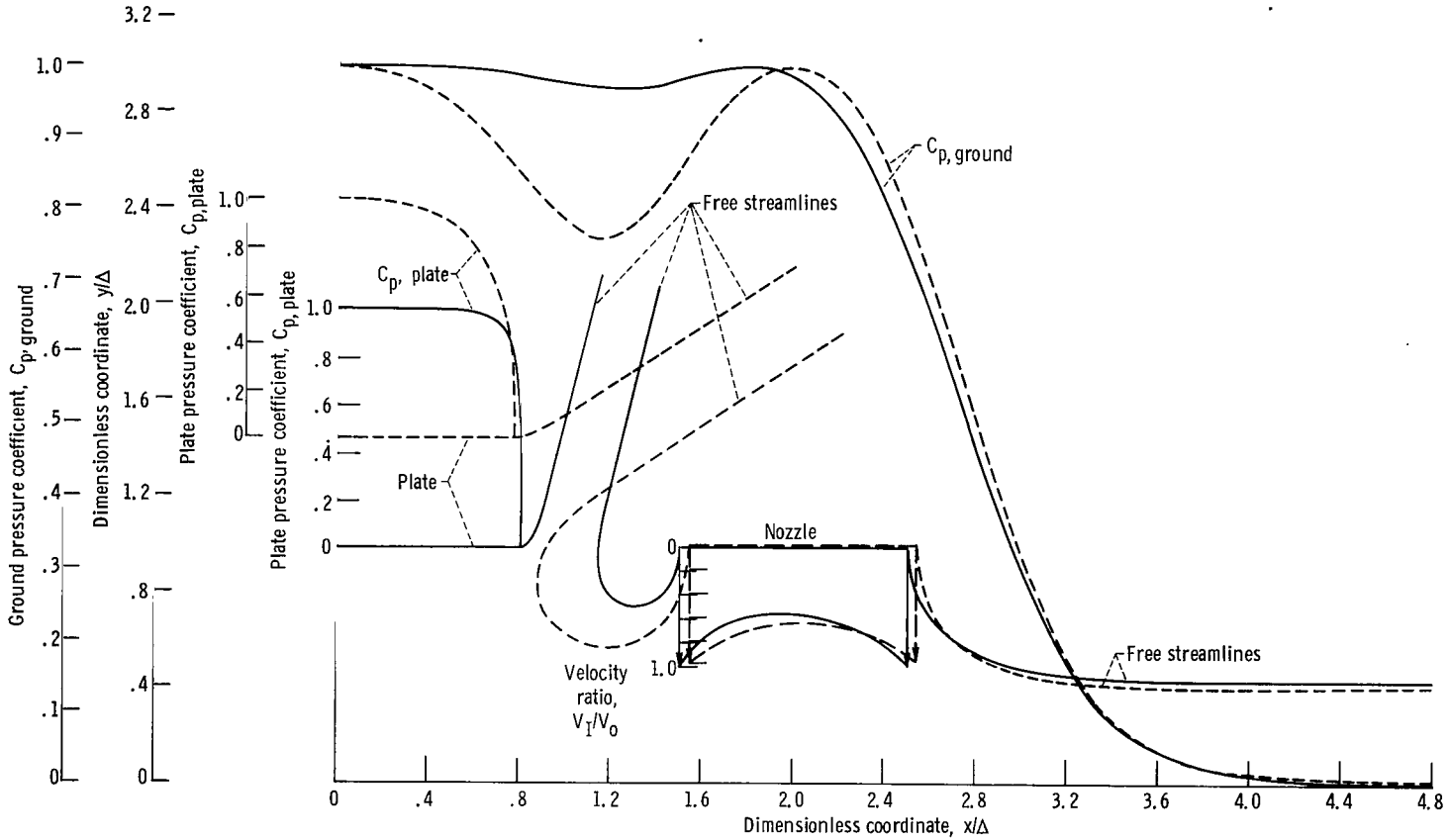

Figure 11. - Effect of plate height for fixed nozzle position.

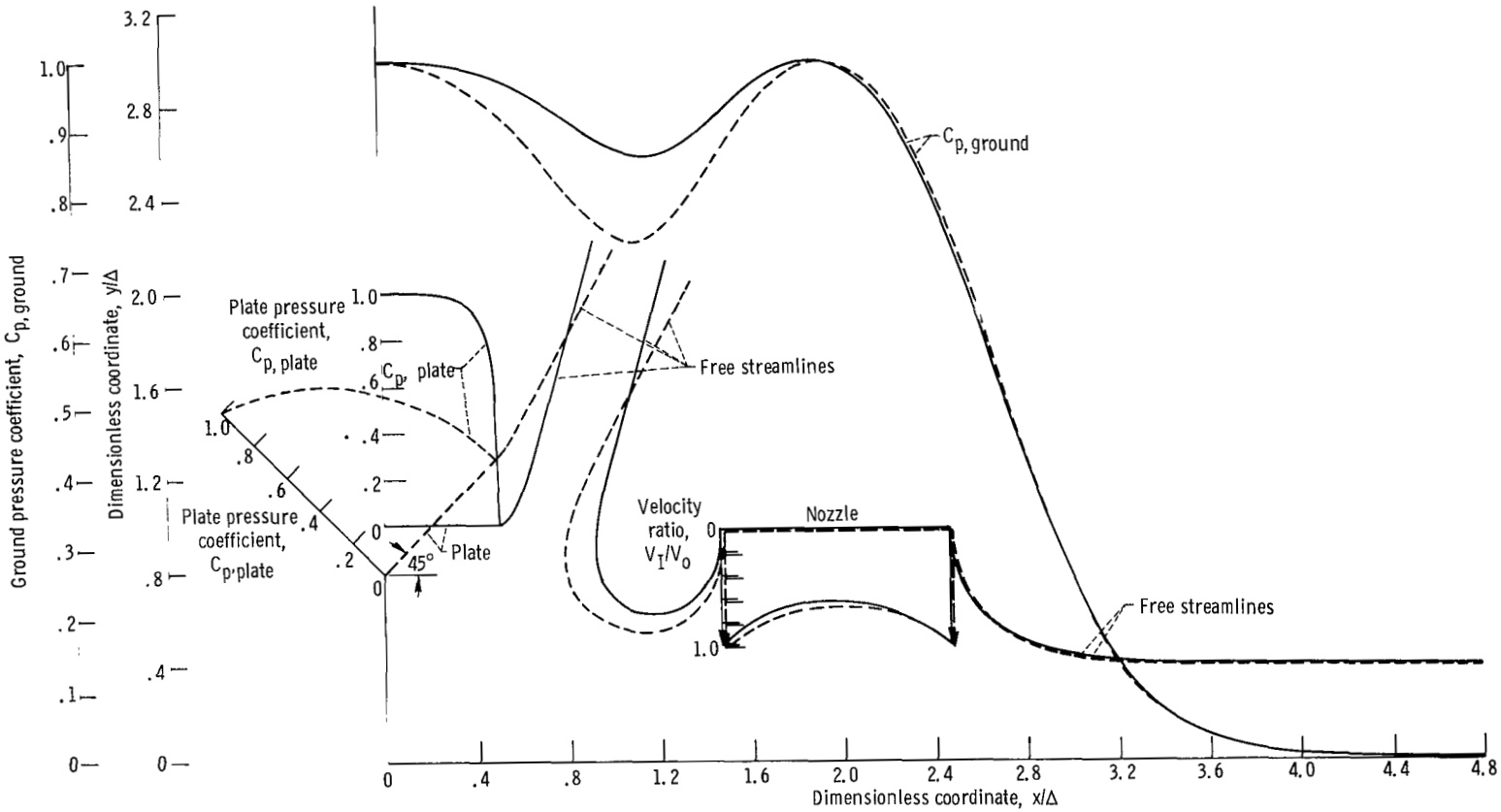

Figure 12. - Effect of plate tilt angle.

In each of figures 10(a) and (b), the plate width is varied while the nozzle is at a fixed position. The (a) and (b) parts are for nozzle heights Y_N = 1 and 2, respectively. For the wider plate the deflection of the left-moving stream is increased and there is a large stagnation region below the plate, especially when the nozzle is in the lower position. As the plate width is increased, the space between the nozzle and plate is diminished, thereby reducing the flow to the left. Raising the plate while keeping the nozzle fixed also increases the jet deflection, as shown in figure 11.

Figure 12 shows the effect of tilting the plate while keeping fixed the horizontal projection of the plate and the nozzle position. The flow pattern is changed only a small amount, the stream flowing to the left being turned more by the tilted plate. The exact shape of the underside of the fuselage is thus of minor importance.

The previous figures have given the reader a quantitative appreciation of the flow trends resulting from varying the five independent parameters governing the flow configuration. The flow patterns can also be used as the zeroth order solution for evaluating entrainment into the flow regions.

Lewis Research Center,
National Aeronautics and Space Administration,
Cleveland, Ohio, March 24, 1969,
129-01-07-07-22.

APPENDIX - WORKING FORMULAS FOR COMPUTING FLOW PATTERN

In this appendix equations (2) and (17) will be rewritten in various forms which are convenient for computing the velocities on and the positions of the various boundaries of the flow. To accomplish this the quantities defined in appendix B of reference 3 will be used. The positions along the free streamlines are found by integrating equation (17) along the sides of the rectangle of figure 7 where $T = i\eta \pm K$. By using the various formulas for the change of argument of elliptic functions, the following relation is obtained in which the elliptic functions depend on real arguments:

$$\left(\frac{dW}{dT}\right)_{T=i\eta\pm K} = \frac{i\overline{V}_I \Delta}{\pi} k'^2 \left[\frac{sn(\eta_F, k') + \frac{\delta_R}{\delta_L}}{1 + \frac{\delta_R}{\delta_L}}\right] \frac{\left[\pm k\, sn(\xi_H, k) - dn(\eta, k')\right] cn(\eta, k')}{\left[dn(\eta, k') \pm k\right]\left[dn(\eta, k') \mp dn(\eta_F, k')\right]} \tag{A1}$$

Similarly, along the top of the rectangle, which corresponds to the solid boundaries and plane of symmetry,

$$\left(\frac{dW}{dT}\right)_{T=\xi+iK'} = \frac{\overline{V}_I \Delta\, k'k}{\pi} \left[\frac{sn(\eta_F, k') + \frac{\delta_R}{\delta_L}}{1 + \frac{\delta_R}{\delta_L}}\right] \frac{\left[sn(\xi_H, k) - sn(\xi, k)\right] cn(\xi, k)}{\left[1 + sn(\xi, k)\right]\left[k\, sn(\xi, k) - dn(\eta_F, k')\right]} \tag{A2}$$

Using the results and definitions of appendix B of reference 3 and substituting equations (A1) and (A2) in equations (2) and (17) give the following working formulas (note that M was defined in equation (18)):

Position and Corresponding Velocity Along Nozzle Exit

$$\left.\begin{aligned} \frac{x(-K, 0) - x(\xi, 0)}{\Delta} &= \frac{x_D - x}{\Delta} \\ &= M \frac{k'}{\pi} \int_{-K}^{\xi} \frac{\left[1 - k\, sn(\xi_H, k) sn(\xi, k)\right]\left[1 - k\, sn(\xi, k)\right] d\xi}{dn(\xi, k)\left[1 - dn(\eta_F, k') sn(\xi, k)\right] R_H^{(4)}(\xi) \sqrt{R_G^{(4)}(\xi)} \left[R_A^{(4)}(\xi)\right]^{\beta/\pi}} \\ \left|\frac{v(\xi, 0)}{V_o}\right| &= R_H^{(4)}(\xi) \sqrt{R_G^{(4)}(\xi)} \left[R_A^{(4)}(\xi)\right]^{\beta/\pi} \end{aligned}\right\} -K \le \xi \le K \tag{A3}$$

Position and Corresponding Velocity Along Ground

$$\left.\begin{aligned}
\frac{x(\xi, K')}{\Delta} &= \frac{x - x_G}{\Delta} \\
&= \frac{Mkk'}{\pi} \int_{\xi_G}^{\xi} \frac{\left[sn(\xi,k) - sn(\xi_H,k)\right]\left[1 - sn(\xi,k)\right] d\xi}{cn(\xi,k)\left[dn(\eta_F,k') - k\,sn(\xi,k)\right] R_H^{(1)}(\xi) \sqrt{R_G^{(1)}(\xi)\left[R_A^{(1)}(\xi)\right]^{\beta/\pi}}} \\
\frac{u(\xi, K')}{V_o} &= R_H^{(1)}(\xi) \sqrt{R_G^{(1)}(\xi)\left[R_A^{(1)}(\xi)\right]^{\beta/\pi}}
\end{aligned}\right\} \quad -K \le \xi \le \xi_G \qquad \text{(A4)}$$

Position and Corresponding Velocity Along Fuselage

$$\left.\begin{aligned}
\left|\frac{z(\xi + iK') - iy(\xi_A, K')}{\Delta}\right| &= \frac{-Mkk'}{\pi} \\
&\times \int_{\xi_A}^{\xi} \frac{\left[sn(\xi,k) - sn(\xi_H,k)\right]\left[1 - sn(\xi,k)\right] d\xi}{cn(\xi,k)\left[dn(\eta_F,k') - k\,sn(\xi,k)\right] R_H^{(1)}(\xi) \sqrt{-R_G^{(1)}(\xi)\left[-R_A^{(1)}(\xi)\right]^{\beta/\pi}}} \\
\frac{|\xi(\xi + iK')|}{V_o} &= \left[\frac{u^2(\xi, K') + v^2(\xi, K')}{V_o^2}\right]^{1/2} \\
&= -R_H^{(1)}(\xi) \sqrt{-R_G^{(1)}(\xi)\left[-R_A^{(1)}(\xi)\right]^{\beta/\pi}}
\end{aligned}\right\} \quad \xi_A \le \xi \le K \qquad \text{(A5)}$$

Height of Point A on Fuselage Above Ground

$$\frac{y(\xi_A, K')}{\Delta} = \frac{y_A - y_G}{\Delta} = \frac{-Mkk'}{\pi} \times \int_{\xi_G}^{\xi_A} \frac{\left[sn(\xi,k) - sn(\xi_H,k)\right]\left[1 - sn(\xi,k)\right] d\xi}{cn(\xi,k)\left[dn(\eta_F,k') - k\,sn(\xi,k)\right] R_H^{(1)}(\xi) \sqrt{-R_G^{(1)}(\xi)\left[R_A^{(1)}(\xi)\right]^{\beta/\pi}}} \qquad \text{(A6)}$$

Coordinates of Free Streamlines

Define $\Theta^{(i)}$ and $H^{\pm}$ as follows

$$\Theta^{(i)}(\eta) = \frac{\pi}{2} + Q_H^{(i)}(\eta) + \frac{1}{2} Q_G^{(i)}(\eta) + \frac{\beta}{\pi} Q_A^{(i)}(\eta); \qquad i = 3, 4 \tag{A7}$$

$$H^{\pm}(\eta) = \frac{\left[dn(\eta, k') \pm k\, sn(\xi_H, k)\right] cn(\eta, k')}{\left[dn(\eta, k') \mp k\right]\left[dn(\eta, k') \pm dn(\eta_F, k')\right]} \tag{A8}$$

Then the coordinates along the the right free streamline extending between the points D and E are

$$\left.\begin{aligned} \frac{x(-K, \eta) - x(-K, 0)}{\Delta} &= \frac{x - x_D}{\Delta} = \frac{k'^2 M}{\pi} \int_0^{\eta} H^+(\eta) \cos\left[\Theta^{(3)}(\eta)\right] d\eta \\ \frac{y(-K, \eta) - y(-K, 0)}{\Delta} &= \frac{y - y_D}{\Delta} = -\frac{k'^2 M}{\pi} \int_0^{\eta} H^+(\eta) \sin\left[\Theta^{(3)}(\eta)\right] d\eta \end{aligned}\right\} \quad 0 \le \eta \le K' \tag{A9}$$

$$\frac{x(K, K') - x(K, 0)}{\Delta} = \frac{x_B - x_C}{\Delta} = \frac{k'^2}{\pi} M \, \mathcal{P}\!\mathcal{V} \int_0^{K'} H^-(\eta) \cos\left[\Theta^{(4)}(\eta)\right] d\eta - \frac{\delta_L}{\Delta} \sin\left[\Theta^{(4)}(\eta_F)\right] \tag{A10}$$

The last term is the horizontal displacement of the left branch of the jet at infinity.

The coordinates along the free streamline between C and F are

$$\left.\begin{aligned} \frac{x(K, \eta) - x(K, 0)}{\Delta} &= \frac{x - x_C}{\Delta} = \frac{k'^2 M}{\pi} \int_0^{\eta} H^-(\eta) \cos\left[\Theta^{(4)}(\eta)\right] d\eta \\ \frac{y(K, \eta) - y(K, 0)}{\Delta} &= \frac{y - y_C}{\Delta} = -\frac{k'^2 M}{\pi} \int_0^{\eta} H^-(\eta) \sin\left[\Theta^{(4)}(\eta)\right] d\eta \end{aligned}\right\} \quad 0 \le \eta \le \eta_F \tag{A11}$$

The coordinates along the free streamline between B and F are

$$\left.\begin{aligned}
\frac{x(K, K') - x(K, \eta)}{\Delta} &= \frac{x_B - x}{\Delta} = \frac{k'^2}{\pi} M \int_{\eta}^{K'} H^-(\eta) \cos\left[\Theta^{(4)}(\eta)\right] d\eta \\
\frac{y(K, K') - y(K, \eta)}{\Delta} &= \frac{y_B - y}{\Delta} = -\frac{k'^2}{\pi} M \int_{\eta}^{K'} H^-(\eta) \sin\left[\Theta^{(4)}(\eta)\right] d\eta
\end{aligned}\right\} \quad \eta_F < \eta \leq K' \qquad \text{(A12)}$$

REFERENCES

1. Spooner, S. H.: The V/STOL Aircraft Environment. Paper No. 68-GT-40, ASME, Mar. 1968.

2. Kemp, E. D. G.: Studies of Exhaust Gas Recirculation for VTOL Aircraft. Paper No. 67-439, AIAA, July 1967.

3. Goldstein, Marvin E.; and Siegel, Robert: Two Dimensional Inviscid Jet Flow From Two Nozzles at an Angle to a Plane Surface. NASA TN D-5064, 1969.

4. Birkhoff, Garrett; and Zarantonello, E. H.: Jets, Wakes, and Cavities. Academic Press, 1957.

NASA-Langley, 1969 —— 1 E-4903